

Contents lists available at [ScienceDirect](https://www.sciencedirect.com)

# Current Research in Pharmacology and Drug Discovery

journal homepage: [www.journals.elsevier.com/current-research-in-pharmacology-and-drug-discovery](http://www.journals.elsevier.com/current-research-in-pharmacology-and-drug-discovery)



## Scaling approaches for the prediction of human clearance of LNA-i-mir-221: A retrospective validation

Massimiliano Fonsi<sup>a</sup>, Jacques Fulbert<sup>a</sup>, Pierre-Andre Billat<sup>a</sup>, Mariamena Arbitrio<sup>b</sup>, Pierosandro Tagliaferri<sup>c</sup>, Pierfrancesco Tassone<sup>c</sup>, Maria Teresa Di Martino<sup>c,\*</sup>

<sup>a</sup> Charles River Laboratories, 27005, Evreux Cedex, France

<sup>b</sup> Institute of Research and Biomedical Innovation (IRIB), Italian National Council (CNR), 88100, Catanzaro, Italy

<sup>c</sup> Department of Experimental and Clinical Medicine, Magna Graecia University, 88100, Catanzaro, Italy

### ARTICLE INFO

#### Keywords:

LNA-i-miR-221  
Non-coding RNA  
ncRNA  
Antisense oligonucleotide  
Pharmacokinetic  
PK  
Allometric method  
Phase 1 clinical trial

### ABSTRACT

LNA-i-miR-221 is a novel microRNA(miRNA)-221 inhibitor designed for the treatment of human malignancies. It has recently undergone phase 1 clinical trial (P1CT) and early pharmacokinetics (PKs) data in cancer patients are now available. We previously used multiple allometric interspecies scaling methods to draw inferences about LNA-i-miR-221 PKs in humans and estimated the patient dose based on the safe and pharmacodynamic (PD) active dose observed in mice, therefore providing a framework for the definition of safe starting and escalation doses for the P1CT. The preliminary data collected during the P1CT showed that the LNA-i-miR-221 anticipated doses, according to our human PK estimation approach, were indeed well tolerated and effective. PD data demonstrated concentration-dependent downregulation of miR-221 and upregulation of its CDKN1B/p27 and PTEN canonical targets as well as stable disease in 8 (50.0%) patients and partial response in 1 (6.3%) colorectal cancer case. Here, we detail the experimentally evaluated PK parameters of LNA-i-miR-221 in human, using both a non-compartmental and a population PKs approach. The population approach was adequately described by a three-compartments model with first-order elimination. The recorded age, sex and body weight of patients were evaluated as potential covariates. The estimated typical population parameter values were clearance (CL = 200 mL/h/kg), central volume of distribution (V1 = 45 mL/kg), peripheral volume of distribution (V2 = 200 mL/kg, volume of the second peripheral compartment V3 = 930 mL/h/kg) and inter-compartmental clearance (Q2 = 480 mL/h/kg and Q3 = 68 mL/h/kg). Age was found to be a predictor of Q3, with a statistically significant correlation. This work aimed also at retrospectively comparing the measured plasmatic clearance values with those predicted by different allometric scaling approaches. Our comparative analysis showed that the most accurate prediction was achieved by applying the single species allometric scaling approach and that the use of more than one species in allometric scaling to predict therapeutic oligonucleotides PKs would not necessarily generate the best prediction. Finally, our predictive approach was found accurate not only in predicting the main PK parameters in human but suggesting the range of effective and safe dose to be applied in the next clinic phase 2.

### 1. Introduction

The role of miRNAs in cancer has been well depicted, since they may act as oncogenes, promoting tumor development by inhibiting tumor suppressor genes, or as tumor suppressors by regulating oncogenes and/or genes that control cell differentiation. A rising body of evidence indicates that miRNAs are valuable therapeutic targets because of their potential to functionally regulate key oncogenic/tumor suppressor

genes by simultaneous regulation of multiple-related pathways (Caracciolo et al., 2019; Di Martino, Campani, et al., 2014; Di Martino et al., 2012, 2021; Misso et al., 2013; Morelli et al., 2015, 2018; Rossi et al., 2013, 2014). Among several miRNAs, miR-221 has been widely investigated for its steady overexpression in a variety of solid and hematologic malignancies (Di Martino et al., 2016, 2022; Di Martino, Gulla et al., 2014).

With the aim of miR-221 therapeutic targeting, we generated a

\* Corresponding author.

E-mail address: [teresadm@unicz.it](mailto:teresadm@unicz.it) (M.T. Di Martino).

<https://doi.org/10.1016/j.crphar.2024.100197>

Received 25 January 2024; Received in revised form 8 July 2024; Accepted 25 July 2024

Available online 2 August 2024

2590-2571/© 2024 The Author(s). Published by Elsevier B.V. This is an open access article under the CC BY-NC license (<http://creativecommons.org/licenses/by-nc/4.0/>).

Locked Nucleic Acid (LNA)-i-miR-221, a phosphorothioate 13-mer oligonucleotide (PS-ODN), for selective miR-221 inhibition (Di Martino et al., 2013). LNA-i-miR-221 takes advantages of LNA technology and PS backbone resulting in increased seed sequence binding affinity and in vivo nuclease resistance (Di Martino et al., 2013; Di Martino, Gulla et al., 2014; Gulla et al., 2016). LNA-i-miR-221 is an effective agent for targeting miR-221, up-regulates its canonical targets, induces significant anti-tumor activity against multiple myeloma (MM) and other malignancies, and rescues tumor sensitivity to alkylating agents (Santolla et al., 2018).

Preclinical studies demonstrated that LNA-i-miR-221 exerts strong anti-tumor activity, providing the first evidence of its efficacy against MM and other tumors (Di Martino, Gulla, et al., 2014). On this basis, LNA-i-miR-221 has been selected and investigated in the dose-escalation phase 1 clinical trial (P1CT) in humans completed in December 2021 (Tassone et al., 2023).

The need to translate safe No Observed Adverse Effect Level (NOAEL) and pharmacological active doses (PAD) from preclinical species to humans, with the aim of predicting safe starting doses in human, required the development of a pharmacokinetic (PK) model able to forecast the clearance and exposure of the LNA-i-miR-221 oligonucleotide in humans and therefore to anticipate safe human plasma levels in the absence of other human data. We have recently proposed quantitative modelling approaches based on allometry (Di Martino et al., 2019). Our approaches also included the Human Equivalent Dose (HED) estimation to be used as the first dose in human, calculated according to guidelines (EMA/CHMP/SWP/28367/07) and the NOAEL identification. We further extended our investigation also applying different scaling methods, based on available preclinical PKs data.

The clinical study exploratory endpoints were PK and PD profiles of LNA-i-miR-221, as well as we conducted a preliminary investigation of anti-tumor activity, disease control and efficacy. The primary endpoints of the first-in-human clinical study that were the safety of LNA-i-miR-221 and the definition of a phase 2 dose, were completely obtained. As we already reported (Tassone et al., 2023). In fact, during the study no clinically significant changes in vital signs (heart rate and blood pressure) from baseline were noted, as well as no clinically significant changes in physical examination or ECG findings. The patients' Performance Status ECOG scores remained within the range 0–2 during the study. Furthermore, no clinically significant changes from baseline were noted in hematological investigations.

Moreover, the assessment of PD profile of LNA-i-miR-221 treatments, through the evaluations of its direct target miR-221 and CDKN1B (p27) and PTEN transcripts in peripheral blood cells (PBMCs) isolated from patients at pre-dose (day1) and 24 h after the last LNA-miR-221 treatment (day5) showed that the dose-range of drug administered is active for the target/biomarkers modulation.

Finally, analysis of the tumor condition investigated for each patient by CT scan images, in accordance with the RECIST 1.1 criteria showed that eight patients had stable disease (SD) (50.0%) during the study, while seven patients (43.8%) had progressive disease (PD). In conclusion the phase one was successfully completed, the safety profile of drug was confirmed also in humans and even if MTD was not achieved, the dose for phase 2 studies has been established.

In this work, we compare the experimentally measured PK parameters in human with those initially predicted based only on data collected during the preclinical phase studies, retrospectively analyzing and discussing the best predictive approaches and the most sensitive parameters impacting the accuracy in our prediction.

Despite important achievements in predicting PKs in human, there are still open questions, as discussed in this manuscript, that still need to be answered, to achieve a complete mechanistic understanding of the PK and PK/PD behavior of oligonucleotides in vivo.

## 2. Methods

### 2.1. Toxicokinetics evaluation in support of GLP safety assessment and preclinical explorative PK analysis

LNA-i-miR-221 quantification was performed in rat, mouse and monkey plasma by LC-MS/MS analysis, using a GLP validated (rat) or qualified analytical method (mouse and monkey) at Aptuit, as previously described (Franzoni et al., 2018; Gallo Cantafio et al., 2016). The toxicokinetics (TK) evaluation was performed using a non-compartmental analysis on Phoenix WinNonlin software, version 6.4 (Pharsight, Mountain View, CA, USA) at CiToxLAB (currently Charles River). TK parameters were determined from the average concentrations in samples collected from different animals at each time point (sparse sampling model) for rat and mouse PK and from individual animals in the case of monkey PK. A separate TK analysis was performed for each sex and sampling occasion. The standard deviation (SD) and the coefficient of variation (CV%) were calculated to assess inter-individual variability. The absence of quantifiable levels of LNA-i-miR-221 at pre-dose (before the first administration) and in control animals was also evaluated.

### 2.2. Human PK analysis

Serial blood and urine samples were collected on day 1 to day 6 in all patients enrolled in the phase I clinical study ((Tassone et al., 2023) EudraCT 2017-002615-33, ClinTrials.Gov: NCT04811898). Table 1 shows the collection times in five dose-escalation cohorts for LNA-i-miR-221 multiple-dose PKs assessment (0.5, 1, 2, 3, and 5 mg/kg). LNA-i-miR-221 concentrations were determined in human plasma and urines using validated mass spectrometry analytical methods (Franzoni et al., 2020) at Aptuit (with a Lower Limit Of Quantification (LLOQ) of 50 ng/mL). PK parameters were estimated using a non-compartmental approach (Phoenix WinNonlin software; version 8.3, Certara L.P). The analysis was performed from individual concentration-time profiles using the intravenous (i.v.) infusion model (200–202). Where applicable, the following PK parameters were evaluated: time to reach the highest observed concentration ( $T_{max}$ ), the observed highest concentration ( $C_{max}$ ), time of the last quantifiable concentration ( $T_{last}$ ), value of the last observed quantifiable concentration ( $C_{last}$ ), apparent terminal elimination rate ( $\lambda_z$ ), apparent terminal half-life ( $t_{1/2}$ ), area under the curve from 0 to the last quantifiable concentration ( $AUC_{tlast}$ ), dose normalized exposure parameters ( $C_{max}/Dose$ ,  $AUC_{tlast}/Dose$ ), area under the curve extrapolated to infinity ( $AUC_{0-inf}$ ), apparent terminal volume of distribution ( $V_z$ ), apparent volume of distribution at steady state ( $V_{ss}$ ) and apparent clearance (CL).

#### 2.2.1. Population pharmacokinetics (PopPK) analysis

The population PK models were developed using a non-linear mixed effects modelling approach using a maximum likelihood estimator of the population parameters based on the Stochastic Approximation Expectation Maximization (SAEM) algorithm (Monolix software, version 2021R2 – Monolix is a Lixoft product) to describe the population variability in LNA-i-miR-221 PK and the relationship between PK parameters and potential explanatory covariates (e.g., age, weight, gender). Development of the population PK model consisted of building a model using the full dataset (15 subjects, involved in the phase I clinical trial referred above and sampled for PK investigation) and by evaluating the potential correlation among the different variables and the inclusion of covariates. Structural model selection was data driven, based on goodness-of-fit plots (e.g., observed vs. predicted concentrations, conditional weighted residual vs. predicted concentration or time, histograms of individual random effects, successful convergence, plausibility and precision of parameter estimates, maximization of the likelihood (-2LL) function via the minimum Objective Function Value (OFV) and of the Corrected Bayesian Information Criteria (BICc).

**Table 1**

Collection times in five LNA-i-miR-221 dose-escalation cohorts for multiple-dose PKs assessment (0.5, 1, 2, 3, and 5 mg/kg).

	Day 1	Day 2	Day 3	Day 4	Day 5	Day 6
Blood sampling	-predose	-predose	-predose	-predose	-24 h after last infusion	-48 h after last infusion
	-15 min from start infusion	-15 min from start infusion	-EOI	-EOI		
	-EOI (End Of Infusion)	-EOI	-1 h from EOI	-1 h from EOI		
	-30 min from EOI	-30 min from EOI	-2 h from EOI	-2 h from EOI		
	-1 h from EOI	-1 h from EOI	-4 h from EOI	-4 h from EOI		
	-2 h from EOI	-2 h from EOI				
	-4 h from EOI	-4 h from EOI				
Urine sampling <sup>a</sup>	Day 1	Day 2	Day 3	Day 4	Day 5	Day 6
	-predose	-24 h urine collection after EOI	-24 h urine collection from EOI	-24 h urine collection from EOI	-24 h urine collection from EOI	-24 h collection starting 24 h from last infusion
	-6 h from EOI					
	-12 h from EOI					

<sup>a</sup> On day 1 were collected fresh urine samples; from day 2 to day 6 were collected 24- hours urine samples.

Plasma concentration data were evaluated using two- and three-compartment models. Distributions of inter-individual variability (IIV) were assumed to be log-normal and were described by an exponential error model. The residual error model was described by separate concentration-proportional terms.

The model that best described LNA-i-miR-221 PK was a three-compartment linear model with first-order elimination, and was dose-proportional.

Concentrations below quantifiable limit were replaced by the LLOQ value (50 ng/mL) when corresponding to the first LLOQ values after C<sub>max</sub> or excluded from analysis in all the other cases. This option was chosen since the same rule was applied to preclinical and clinical NCA PK analysis, and we wanted to keep the NCA and CA approaches consistent. In addition, we tested the option of letting Monolix

extrapolate the BLQ values (keeping the lower limit of the extrapolated values at 10 ng/mL) and this test didn't produce more precise estimations of the model parameters. Missing drug concentrations were also excluded from the final analysis. Two evident outlier values were excluded from the analysis: time 72.5 h (h) from individual 14 and time 50.5 h from individual 19. Peak concentrations in plasma were observed immediately after dosing in most cases; on five separate instances T<sub>max</sub> was seen later. These observations were left in the dataset as likely due to analytical variability and contributed generating some marginal misalignment between experimental and predicted confidential intervals in the visual predictive check (VPC, Fig. 1).

Investigation of correlation among parameters or covariate-parameter relationships was based on the range of covariate values in the dataset, mechanistic plausibility and exploratory graphics (i.e.

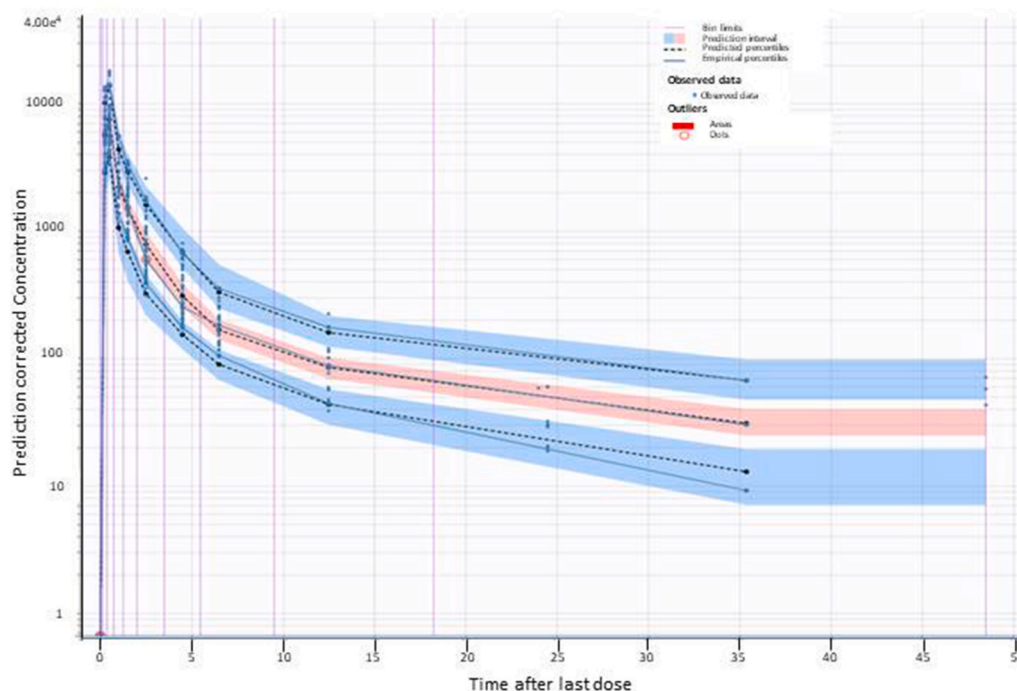


**Fig. 1.** Prediction corrected visual predictive check vs. time after last dose for the final model for LNA-i-miR-221. Prediction intervals for each percentile are estimated across all simulated data and displayed as colored areas (pink for the 50th percentile, blue for the 10th and 90th percentiles). Prediction intervals are computed with a level of 90%. Empirical percentiles: percentiles of the observed data, calculated each unique value of time (bins, bin intervals are defined by vertical violet lines). Outliers are highlighted with red dots and areas. (For interpretation of the references to color in this figure legend, the reader is referred to the Web version of this article.)

correlation between different parameters and between parameter and covariate values in the population). Correlation among parameters and with potential covariates were considered for inclusion in the model if the parameters were significantly correlated [ $R^2 \geq 0.7$  or  $p\text{value} < 0.05$ ] (Fig. 2A–B) and if a decrease in OFV/BICc was observed by including these correlations in the model.

Correlation among CL, Q1, V2, Q3 and V3 were included in the final model. The only covariate included in the model was Logt Age =  $(\log(\text{Age}/62.4438))$  which showed a strong correlation with V1 parameter (Fig. 3)

The simulated LNA-i-miR-221 concentrations with prediction correction (pcVPC), where both the observed and the simulated concentrations were normalized by the ratio between the median typical population predictions for the specific time bin and the typical population prediction for the observation, were summarized at the 5th percentile, median and 95th percentile, and the 90th prediction interval around each percentile was calculated.

### 3. Results

#### 3.1. PKs of LNA-i-miR-221 in humans

##### 3.1.1. Non compartmental analysis (NCA)

The experimentally measured clearance (CL) values in human NCA are summarized in Table 2. Values are grouped per dose level and subject. As no significant differences were observed in the calculated PK parameters across the different PK sampling occasions (i.e. after single or repeated administration, up to four daily administrations) all the different occasions have been grouped and were used to estimate the

relative descriptive statistic parameters for each individual dose level. The PK profiles of LNA-i-miR-221 following administration of intravenous (i.v.) doses ranging from 0.5 mg/kg to 5 mg/kg are presented in Fig. 4.

In the dose-escalation cohorts, LNA-i-miR-221 was rapidly cleared from the plasma compartment and distributed into tissues at all dose levels. The highest blood concentration was observed as expected after i. v. administration, i.e. at the end of the infusion, with a few exceptions when  $T_{\text{max}}$  was observed 15 min later, probably due to analytical variability as, in these cases, concentrations were close to those observed at the end of infusion. On the four occasions in all cohorts, LNA-i-miR-221 plasma terminal half-life harmonic mean values ranged from 1.1 to 4.9 hours. The inferior extreme values in this range, observed at lower doses, probably do not represent the true terminal half-life but more probably the half-life of the initial distribution/elimination mixed phase, as also suggested by the results of LNA-i-miR-221 analysis in urines (detectable levels were observed until the last collected samples at the lowest dose (0.5 mg/kg) i.e. 24h–48h interval after the end of infusion occurred on day 4 (Tassone et al., 2023)). Similarly, the apparent terminal volume of distribution ( $V_z$ ) calculated from the plasma profile may not represent the true terminal value, especially at the lower dose. Indeed, the observed apparent  $V_z$  in humans, with values in the range of 0.2–2.0 L/kg (Table 2), relatively constant across the different sampling occasions in the same dose cohort, also increased with the dose).  $V_z$  in human was in general significantly lower (<2-folds) than the values measured after single i.v. administration in rat (2.6 L/kg) and monkey (3.3 L/kg) (Di Martino et al., 2019). This difference is, in part, attributable to the bioanalytical sensitivity (LLOQ = 50 ng/mL in both human plasma and urines) and to the lower doses

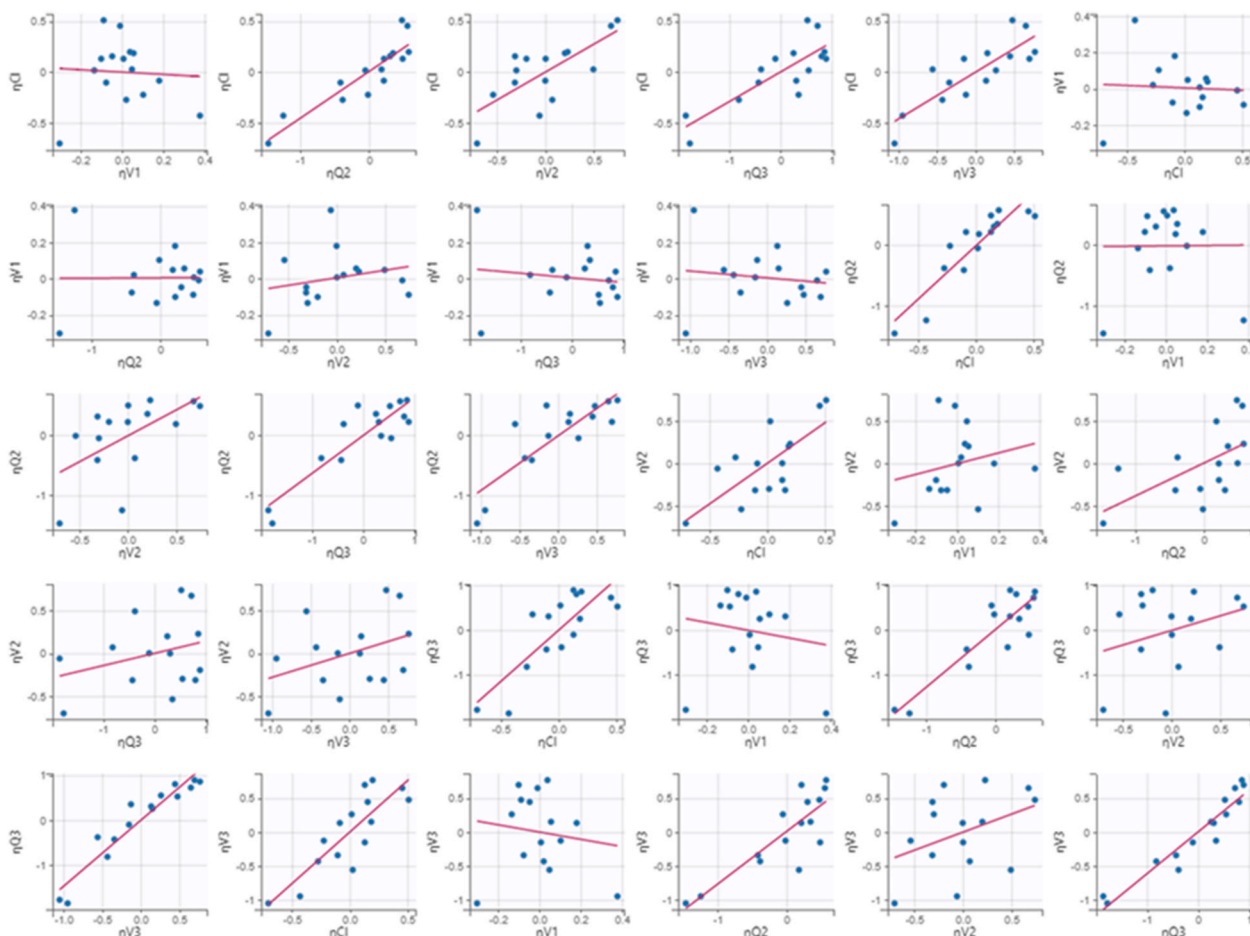


Fig. 2. A) Correlation among population parameters. B) Correlation between population parameters and ages and body weight covariates.



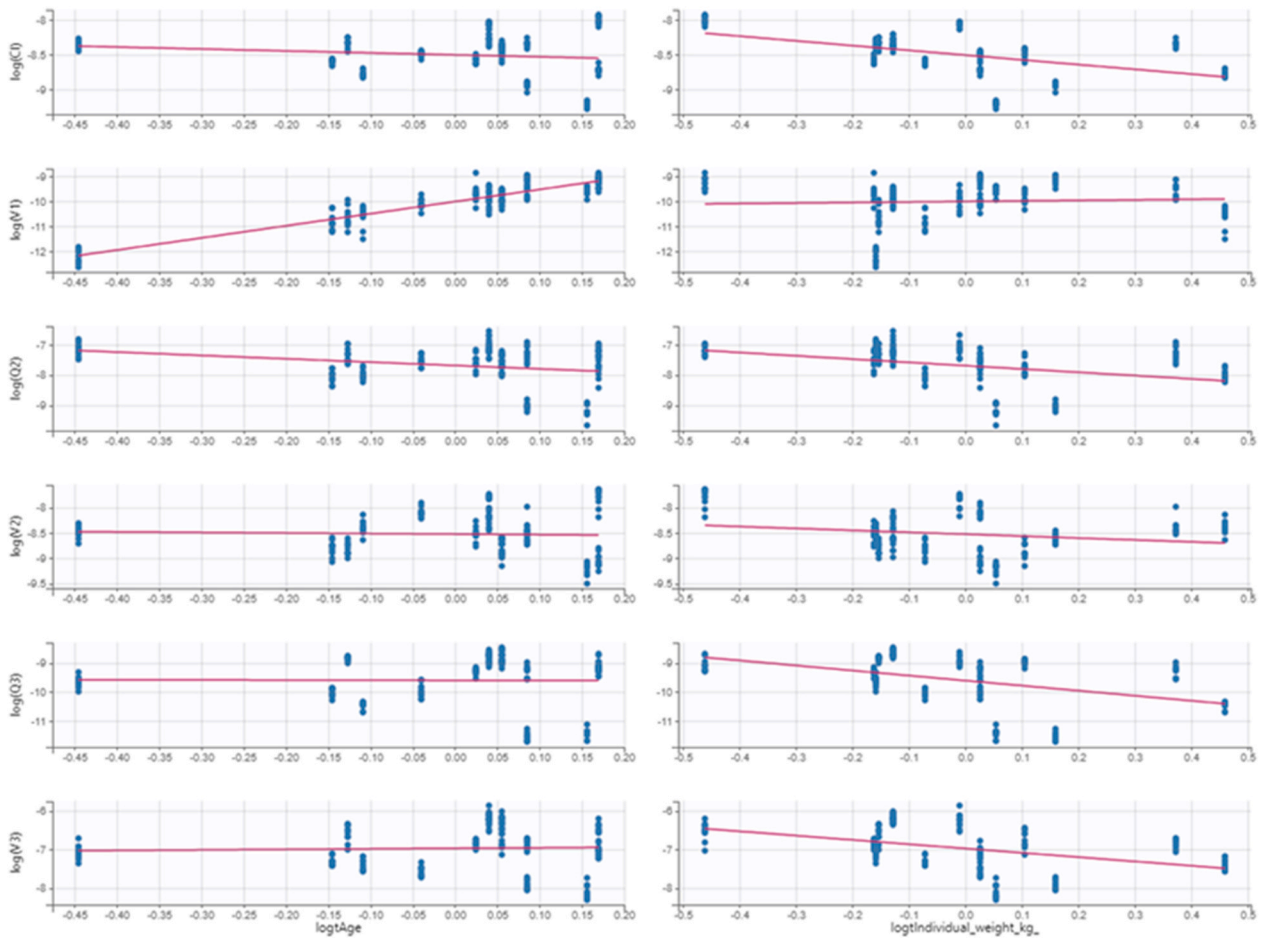


Fig. 2. (continued).

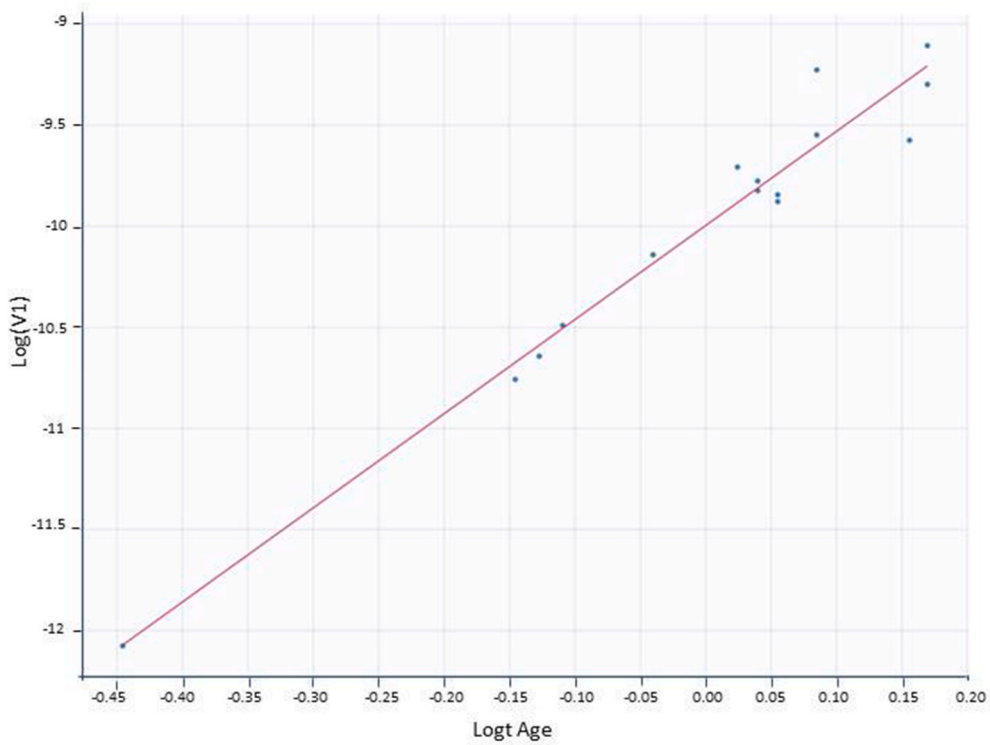


Fig. 3. Correlation between logtAge and log V1 ( $R^2 = 0.98$ ).

**Table 2**  
Averaged plasma PK parameters of LNA-i-miR-221 calculated from Phase 1 clinical trial patients.

Occasion	Subject_identifier	Dose_Level	cohort	Lambda_z	HL_Lambda_z	Tmax	Cmax	Cmax_D	Tlast	Clast	AUClast	AUCINF_obs	AUC_% Extrap_obs	Vz_obs	Cl_obs	Vss_obs	AUClast_Dose
				(1/h)	(h)	(h)	(ng/ mL)	(kg*ng/ mL/mg)	(h)	(ng/ mL)	(h*ng/ mL)	(h*ng/mL)	(%)	(mL/ kg)	(mL/ h/kg)	(mL/ kg)	(h*ng/mL)/ (mg/kg)
Day 1	2	0.5	1	0.362	1.917	0.5	2029	4057	6.5	63	2341	2516	7	550	199	399	4682
Day 1	4	0.5	1	0.654	1.060	0.5	1947	3893	4.5	55	1832	1916	4	399	261	262	3665
Day 1	5	0.5	1	1.060	0.654	0.5	2221	4441	2.5	87	1508	1591	5	296	314	193	3016
Day 2	2	0.5	1	0.367	1.890	0.5	2150	4310	6.5	60	2540	2700	6	326	190	326	5080
Day 2	4	0.5	1	1.020	0.680	0.25	1886	3770	2.5	113	1546	1660	7	296	302	205	3092
Day 4	5	0.5	1	0.612	1.130	0.5	2180	4370	4.5	52	1670	1750	5	278	285	278	3340
Day 3	2	0.5	1	0.529	1.311	0.5	2237	4474	4.5	99	2394	2581	7	366	194	270	4788
Day 3	4	0.5	1	–	–	0.5	1888	3775	2.5	137	1472	–	–	–	340	–	2943
Day 3	5	0.5	1	–	–	0.5	1686	3372	2.5	105	1378	–	–	–	362	–	2755
Day 4	2	0.5	1	0.663	1.045	0.5	1930	3860	4.5	64	2085	2181	4	346	229	272	4170
Day 4	4	0.5	1	0.532	1.304	0.5	1965	3929	4.5	78	2003	2149	7	438	233	311	4006
Day 4	5	0.5	1	–	–	0.5	1684	3368	2.5	86	1296	–	–	–	385	–	2592
			<b>Mean</b>	<b>0.644</b>	<b>1.22</b>	<b>0.48</b>	<b>1983</b>	<b>3968</b>	<b>4.0</b>	<b>83</b>	<b>1839</b>	<b>2116</b>	<b>6</b>	<b>366</b>	<b>274</b>	<b>280</b>	<b>3677</b>
			SD	0.250	0.45	0.07	188	379	1.5	26	427	415	1	86	67	62	854
			Min	0.362	0.654	0.25	1684	3368	2.5	52.4	1296	1591	4	278	190	193	2592
			<b>Median</b>	<b>0.612</b>	<b>1.130</b>	<b>0.5</b>	<b>1956</b>	<b>3911</b>	<b>4.5</b>	<b>81.6</b>	<b>1751</b>	<b>2149</b>	<b>6</b>	<b>346</b>	<b>273</b>	<b>272</b>	<b>3502</b>
			Max	1.060	1.917	0.5	2237	4474	6.5	137.1	2540	2700	7	550	385	399	5080
			CV%	39	37	15	9	10	38	32	23	20	19	24	25	22	23
			Harmonic Mean	0.568	1.076	0.462	1966.6	3934	3.5	76	1752	2044	6	351	259	267	3504
			Geometric Mean	0.604	1.147	0.472	1975.1	3951	3.7	80	1794	2080	6	358	267	273	3589
Occasion	Subject_identifier	Dose_Level	cohort	Lambda_z	HL_Lambda_z	Tmax	Cmax	Cmax_D	Tlast	Clast	AUClast	AUCINF_obs	AUC_% Extrap_obs	Vz_obs	Cl_obs	Vss_obs	AUClast_Dose
				(1/h)	(h)	(h)	(ng/ mL)	(kg*ng/ mL/mg)	(h)	(ng/ mL)	(h*ng/ mL)	(h*ng/mL)	(%)	(mL/ kg)	(mL/ h/kg)	(mL/ kg)	(h*ng/mL)/ (mg/kg)
Day 1	6	1	2	0.460	1.507	0.25	2525	2525	6.5	118	4098	4355	6	499	230	420	4098
Day 1	7	1	2	0.483	1.435	0.5	3516	3516	6.5	72	3459	3608	4	574	277	392	3459
Day 1	9	1	2	0.345	2.011	0.25	3087	3087	6.5	77	3160	3382	7	858	296	461	3160
Day 2	6	1	2	0.315	2.199	0.25	3797	3797	6.5	116	3981	4348	8	730	230	467	3981
Day 2	7	1	2	0.354	1.961	0.5	2186	2186	6.5	66	2605	2791	7	1014	358	654	2605
Day 2	9	1	2	0.260	2.667	0.5	3376	3376	6.5	85	3592	3920	8	981	255	463	3592
Day 3	6	1	2	0.539	1.286	0.5	3309	3309	4.5	181	3953	4289	8	433	233	346	3953
Day 3	7	1	2	0.588	1.180	0.5	2102	2102	4.5	97	2453	2619	6	650	382	523	2453
Day 3	9	1	2	0.444	1.562	0.5	2557	2557	4.5	120	2560	2831	10	796	353	539	2560
Day 4	6	1	2	0.639	1.084	0.5	2031	2031	4.5	90	2435	2576	5	607	388	502	2435
Day 4	7	1	2	0.531	1.306	0.5	2732	2732	4.5	101	2713	2904	7	649	344	452	2713
Day 4	9	1	2	0.484	1.433	0.5	2459	2459	4.5	108	2488	2712	8	762	369	526	2488
			<b>Mean</b>	<b>0.453</b>	<b>1.64</b>	<b>0.44</b>	<b>2806</b>	<b>2806</b>	<b>5.5</b>	<b>103</b>	<b>3125</b>	<b>3361</b>	<b>7</b>	<b>713</b>	<b>310</b>	<b>479</b>	<b>3125</b>
			SD	0.115	0.47	0.11	595	595	1.0	31	660	713	2	180	63	79	660
			Min	0.260	1.084	0.25	2031	2031	4.5	66	2435	2576	4	433	230	346	2435
			<b>Median</b>	<b>0.471</b>	<b>1.471</b>	<b>0.5</b>	<b>2645</b>	<b>2645</b>	<b>5.5</b>	<b>99</b>	<b>2937</b>	<b>3143</b>	<b>7</b>	<b>690</b>	<b>320</b>	<b>465</b>	<b>2937</b>
			Max	0.639	2.667	0.5	3797	3797	6.5	181	4098	4355	10	1014	388	654	4098
			CV%	25	29	26	21	21	19	30	21	21	22	25	20	17	21
			Harmonic Mean	0.424	1.529	0.400	2693.2	2693	5.3	96	3004	3230	7	671	298	467	3004
			Geometric Mean	0.439	1.579	0.420	2749.1	2749	5.4	99	3063	3294	7	692	304	473	3063

Occasion	Subject_identifier	Dose_Level	cohort	Lambda_z	HL_Lambda_z	Tmax	Cmax	Cmax_D	Tlast	Clast	AUClast	AUCINF_obs	AUC_% Extrap_obs	Vz_obs	Cl_obs	Vss_obs	AUClast_Dose
				(1/h)	(h)	(h)	(ng/ mL)	(kg*ng/ mL/mg)	(h)	(ng/ mL)	(h*ng/ mL)	(h*ng/mL)	(%)	(mL/ kg)	(mL/ h/kg)	(mL/ kg)	(h*ng/mL)/ (mg/kg)
Day 1	10	2	3	0.479	1.446	0.5	6248	3124	6.5	164	7190	7533	5	554	265	402	3595
Day 1	11	2	3	0.396	1.749	0.5	4244	2122	6.5	116	5049	5342	5	944	374	649	2524
Day 1	12	2	3	0.574	1.208	0.5	9421	4710	6.5	145	10458	10710	2	325	187	218	5229
Day 2	10	2	3	0.360	1.927	0.5	6579	3290	6.5	148	7549	7961	5	698	251	386	3775
Day 2	11	2	3	0.297	2.334	0.5	5542	2771	6.5	141	5569	6042	8	1114	331	609	2784
Day 2	12	2	3	0.547	1.267	0.25	14499	7250	6.5	145	10603	10869	2	336	184	193	5302
Day 3	10	2	3	0.534	1.297	0.5	4959	2480	4.5	257	5770	6251	8	599	320	470	2885
Day 3	11	2	3	0.510	1.360	0.5	4728	2364	4.5	178	4639	4987	7	787	401	539	2319
Day 3	12	2	3	0.601	1.153	0.5	8162	4081	4.5	232	7715	8101	5	411	247	280	3857
Day 4	10	2	3	0.539	1.286	0.5	5659	2830	4.5	257	6177	6654	7	558	301	418	3089
Day 4	11	2	3	0.511	1.357	0.5	4310	2155	4.5	178	4325	4673	7	838	428	575	2162
Day 4	12	2	3	0.529	1.310	0.5	4340	2170	4.5	170	4484	4805	7	787	416	572	2242
			<b>Mean</b>	<b>0.490</b>	<b>1.47</b>	<b>0.48</b>	<b>6558</b>	<b>3279</b>	<b>5.5</b>	<b>178</b>	<b>6627</b>	<b>6994</b>	<b>6</b>	<b>663</b>	<b>309</b>	<b>443</b>	<b>3314</b>
			SD	0.092	0.35	0.07	2969	1485	1.0	47	2158	2127	2	244	85	154	1079
			Min	0.297	1.153	0.25	4244	2122	4.5	116	4325	4673	2	325	184	193	2162
			<b>Median</b>	<b>0.520</b>	<b>1.334</b>	<b>0.5</b>	<b>5601</b>	<b>2800</b>	<b>5.5</b>	<b>167</b>	<b>5974</b>	<b>6453</b>	<b>6</b>	<b>649</b>	<b>310</b>	<b>444</b>	<b>2987</b>
			Max	0.601	2.334	0.5	14499	7250	6.5	257	10603	10869	8	1114	428	649	5302
			CV%	19	24	15	45	45	19	26	33	30	34	37	27	35	33
			Harmonic Mean	0.470	1.415	0.462	5774.7	2887	5.3	168	6080	6477	5	575	286	381	3040
			Geometric Mean	0.481	1.442	0.472	6104.0	3052	5.4	172	6336	6721	5	619	298	414	3168
Occasion	Subject_identifier	Dose_Level	cohort	Lambda_z	HL_Lambda_z	Tmax	Cmax	Cmax_D	Tlast	Clast	AUClast	AUCINF_obs	AUC_% Extrap_obs	Vz_obs	Cl_obs	Vss_obs	AUClast_Dose
				(1/h)	(h)	(h)	(ng/ mL)	(kg*ng/ mL/mg)	(h)	(ng/ mL)	(h*ng/ mL)	(h*ng/mL)	(%)	(mL/ kg)	(mL/ h/kg)	(mL/ kg)	(h*ng/mL)/ (mg/kg)
Day 1	13	3	4	0.435	1.595	0.5	12030	4010	6.5	129	11846	12143	2	568	247	265	3949
Day 1	14	3	4	0.282	2.459	0.5	24212	8071	12.5	114	29652	30055	1	354	100	181	9884
Day 1	15	3	4	0.211	3.287	0.25	6362	2121	12.5	64	8531	8833	3	1610	340	822	2844
Day 2	13	3	4	0.138	5.039	0.25	9712	3237	12.5	98	12621	13333	5	1636	225	559	4207
Day 2	14	3	4	0.125	5.527	0.5	23313	7771	24.5	51	30013	30423	1	786	99	275	10004
Day 2	15	3	4	0.149	4.660	0.5	6001	2000	12.5	78	7731	8256	6	2443	363	1097	2577
Day 3	13	3	4	0.718	0.966	0.5	11054	3685	4.5	292	11467	11874	3	352	253	276	3822
Day 3	14	3	4	0.154	4.501	0.5	25346	8449	24.5	71	34302	34760	1	560	86	290	11434
Day 3	15	3	4	0.475	1.458	0.5	5802	1934	4.5	311	6443	7098	9	889	423	662	2148
Day 4	13	3	4	0.681	1.017	0.5	11164	3721	4.5	239	10149	10500	3	419	286	283	3383
Day 4	14	3	4	0.170	4.077	0.5	199083	66361	24.5	81	120225	120703	0.4	146	25	32	40075
Day 4	15	3	4	0.496	1.398	0.5	8624	2875	4.5	345	8515	9212	8	657	326	448	2838
			<b>Mean</b>	<b>0.336</b>	<b>3.00</b>	<b>0.46</b>	<b>28558</b>	<b>9519</b>	<b>12.3</b>	<b>156</b>	<b>24291</b>	<b>24766</b>	<b>4</b>	<b>868</b>	<b>250</b>	<b>432</b>	<b>8097</b>
			SD	0.217	1.71	0.10	54179	18060	8.1	109	31781	31772	3	681	127	302	10594
			Min	0.125	0.966	0.25	5802	1934	4.5	51	6443	7098	0	146	25	32	2148
			<b>Median</b>	<b>0.246</b>	<b>2.873</b>	<b>0.5</b>	<b>11109</b>	<b>3703</b>	<b>12.5</b>	<b>106</b>	<b>11656</b>	<b>12009</b>	<b>3</b>	<b>613</b>	<b>250</b>	<b>287</b>	<b>3885</b>
			Max	0.718	5.527	0.5	199083	66361	24.5	345	120225	120703	9	2443	423	1097	40075
			CV%	65	57	21	190	190	66	70	131	128	73	78	55	70	131
			Harmonic Mean	0.231	2.062	0.429	10840.3	3613	8.1	104	12331	12990	2	500	121	194	4110
			Geometric Mean	0.277	2.507	0.445	14383.7	4795	10.0	126	15739	16366	3	663	183	326	5246
Occasion	Subject_identifier	Dose_Level	cohort	Lambda_z	HL_Lambda_z	Tmax	Cmax	Cmax_D	Tlast	Clast	AUClast	AUCINF_obs	AUC_% Extrap_obs	Vz_obs	Cl_obs	Vss_obs	AUClast_Dose

(continued on next page)

Table 2 (continued)

Occasion	Subject_identifier	Dose_Level	cohort	Lambda_z	HL_Lambda_z	Tmax	Cmax	Cmax_D	Tlast	Clast	AUClast	AUCINF_obs	AUC_% Extrap_obs	Vz_obs	Cl_obs	Vss_obs	AUClast Dose
				(1/h)	(h)	(h)	(ng/ mL)	(kg*ng/ mL/mg)	(h)	(ng/ mL)	(h*ng/ mL)	(h*ng/mL)	(%)	(mL/ kg)	(mL/ h/ kg)	(mL/ kg)	(h*ng/ mL)/ (mg/kg)
				(1/h)	(h)	(h)	(ng/ mL)	(kg*ng/ mL/mg)	(h)	(ng/ mL)	(h*ng/ mL)	(h*ng/mL)	(%)	(mL/ kg)	(mL/ h/ kg)	(mL/ kg)	(h*ng/ mL)/ (mg/kg)
Day 1	18	5	5	0.121	5.709	0.25	18034	3607	24.5	58	24167	24643	2	1671	203	693	4833
Day 1	19	5	5	0.116	5.957	0.25	22074	4415	24.5	63	28536	29078	2	1478	172	529	5707
Day 1	21	5	5	0.215	3.231	0.25	24901	4980	12.5	264	34031	35263	3	661	142	365	6806
Day 2	18	5	5	0.102	6.781	0.5	18045	3609	24.5	87	26048	26897	3	1819	186	762	5210
Day 2	19	5	5	0.130	5.318	0.25	31271	6254	24.5	90	36424	37118	2	1033	135	414	7285
Day 2	21	5	5	0.167	4.157	0.5	23787	4757	24.5	51	36519	36827	1	814	136	370	7304
Day 3	18	5	5	0.146	4.737	0.5	12448	2490	24.5	78	25066	25596	2	1335	195	899	5013
Day 3	19	5	5	–	–	2.5	75397	15079	24.5	123	103022	–	–	–	49	–	20604
Day 3	21	5	5	0.167	4.147	0.5	23303	4661	24.5	76	39079	39533	1	757	126	465	7816
Day 4	18	5	5	0.154	4.507	0.5	13831	2766	24.5	78	28232	28736	2	1131	174	786	5646
Day 4	19	5	5	0.069	9.994	0.5	18096	3619	48.5	66	34477	35423	3	2035	141	1080	6895
Day 4	21	5	5	0.160	4.340	0.5	26610	5322	24.5	86	40628	41164	1	761	121	453	8126
			<b>Mean</b>	<b>0.141</b>	<b>5.35</b>	<b>0.58</b>	<b>25650</b>	<b>5130</b>	<b>25.5</b>	<b>93</b>	<b>38019</b>	<b>32752</b>	<b>2</b>	<b>1227</b>	<b>157</b>	<b>620</b>	<b>7604</b>
			SD	0.039	1.83	0.62	16560	3312	8.0	57	21224	5888	1	474	42	239	4245
			Min	0.069	3.231	0.25	12448	2490	12.5	51	24167	24643	1	661	49	365	4833
			<b>Median</b>	0.146	4.737	<b>0.5</b>	22689	4538	<b>24.5</b>	78	34254	35263	2	1131	141	529	6851
			Max	0.215	9.994	2.5	75397	15079	48.5	264	103022	41164	3	2035	203	1080	20604
			CV%	28	34	106	65	65	31	61	56	18	41	39	27	39	56
			Harmonic Mean	0.129	4.926	0.395	20979.2	4196	23.6	78	33034	31765	2	1069	130	545	6607
			Geometric Mean	0.135	5.119	0.454	22765.9	4553	24.5	84	34882	32260	2	1145	141	580	6976

not calculated.

CL extrapolated using AUClast suspected outlier, excluded from statistics.

italic.

underscored.



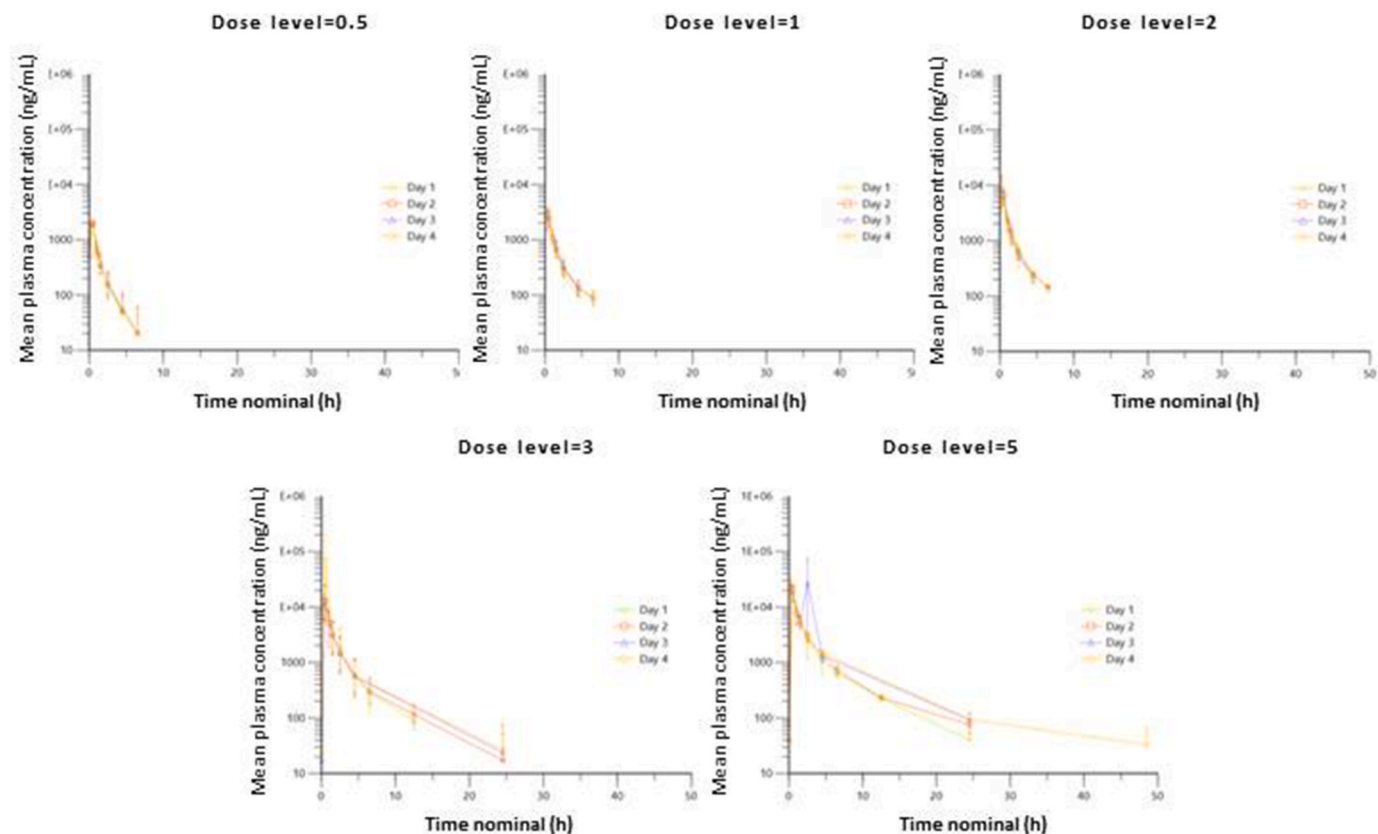


Fig. 4. PK profiles at each different sampling day. Profiles were grouped according to each different dose levels ranging from 0,5 to 5 mg/kg.

used in the clinical protocol compared to those used in the preclinical phase. These two combined factors did not always permit to precisely profile the true terminal half-life in human. This is also evident in the comparison of the last quantifiable time points in man with those observed in preclinical species: i.e. 4h (median value) after the end of infusion in man at the low dose (0.5 mg/kg), 24h at the highest dose (5 mg/kg), while  $t_{last}$  was 24h post end of infusion both in rats (starting from the lowest tested dose: 5 mg/kg) and in monkeys (8.75 mg/kg).

No significant differences were observed during the treatment period in terms of plasma exposure parameters (comparing both  $C_{max}$  and  $AUC_{tlast}$  on four occasions). This also suggests that no evident changes in systemic clearance during the repeated treatment interval occurred. The summarized plasma parameters including  $C_{max}$ ,  $T_{max}$ ,  $AUC_{tlast}$ ,  $AUC_{tlast}/dose$ ,  $T_{1/2}$ ,  $Cl$  and  $V_z$  are presented in Table 2.

Interestingly, the NCA results obtained in plasma seems to indicate, on average, an apparent non-linear pharmacokinetics over the range of doses explored in this clinical trial. A more than dose-proportional increase in LNA-i-miR-221 plasma exposure was observed based on  $AUC_{tlast}/dose$  at 0,5 and 5 mg/kg (the averaged values for this parameter doubled between 0.5 and 5 mg/kg). Similar findings were also observed in rats during the preclinical safety assessment, in which the explored range of doses (5, 12.5 and 125 mg/kg) was necessarily higher than those administered in the actual clinical phase. Following the first administration in rats, the increase of the dose from 5 to 125 (25-fold) and from 12.5 to 125 mg/kg (10-fold) produced an increase in  $AUC_{0-24h}$  of 39.5- and 15.9-folds, respectively. On day 18 (cycle 2), the increase in  $AUC_{0-24h}$  between the doses of 5 and 12.5 mg/kg was ~3.4-folds, while between 5 and 125 and 12.5 and 125 mg/kg it was 68.9- and 20.5-folds, respectively (Di Martino et al., 2020). The measured average clearance values were, respectively: 604, 436 and 284 mL/min/kg, at 5, 12.5 and 125 mg/kg (male and females, including all the sampling occasions). Similarly, the calculated terminal volume of distribution in rats also appeared to be dose dependent, decreasing as the dose increased (Di

Martino et al., 2020).

At least part of this difference may be explained with the bio-analytical method sensitivity that didn't let precisely estimate the terminal half-life of the drug at lower dosing regimens, with consequent underestimation of the  $AUC_{inf}$  values at lower doses. This hypothesis is strongly supported by the compartmental analysis in humans, as discussed in the next section.

### 3.2. PopPK analysis results

Patient population was represented by 5 males and 10 females, the range of patients age span from 40 to 74 years with a median value of 65 years. Body weight ranged between 43 and 108 kg, with a median value of 67.5 kg.

Parameter estimates for the final model are shown in Table 3a–b. The estimated typical population parameter values were: clearance (CL) = 200 mL/h/kg with individual values ranging from 100 to 340 mL/h/kg, central volume of distribution ( $V_1$ ) = 45 mL/kg, this value should correspond to the blood compartment were the drug is initially directly administered and before diffusing in other organs, peripheral volume of distribution ( $V_2$ ) = 200 mL/kg, volume of the second peripheral compartment ( $V_3$ ) = 930 mL/h/kg, inter-compartmental clearance  $Q_2$  = 480 mL/h/kg, and  $Q_3$  = 68 mL/h/kg.

Interestingly, the PopPK analysis does not support the hypothesis of a non-linear CL (the corresponding model was tested but the OFV and BIC scores and the pcVPC were worst respect to the linear CL model). This finding seems to confirm then that the apparent dose dependent CL values observed in the NCA analysis was the consequence of the limited sensitivity of the analytical method.

An estimation of the terminal volume of distribution, calculated as  $V_1+V_2+V_3$ , is very close to the  $V_z$  parameter estimated by NCA at larger doses. Similarly, the terminal half-life based on these results, estimated in a first approximation as  $\ln 2 \cdot (V_1+V_2+V_3)/CL$ , indicates a

**Table 3a**

Predicted population PK parameter values for LNA-i-miR-221 in human (n = 15 subjects), including relative standard errors percent (RSE%).

	VALUE	STOCH. APPROX.	
		S.E.	R.S.E.(%)
<b>Fixed Effects</b>			
Cl_pop	200	16	8.09
V1_pop	45	26	58.2
beta_V1_logtAge	4.67	2.32	49.7
Q2_pop	480	130	27.3
V2_pop	200	32	16.4
Q3_pop	68	16	22.7
V3_pop	930	150	16.3
<b>Standard Deviation of the Random Effects</b>			
omega_Cl	0.31	0.081	26.2
omega_V1	0.31	0.22	71.3
omega_Q2	0.61	0.2	32.3
omega_V2	0.43	0.12	28.6
omega_Q3	0.85	0.28	32.5
omega_V3	0.58	0.18	31.5
<b>Correlations</b>			
corr_Q2_Cl	0.85	0.11	12.7
corr_Q3_Cl	0.78	0.18	23.2
corr_V2_Cl	0.69	0.19	27.3
corr_V3_Cl	0.78	0.16	20.5
corr_Q3_Q2	0.83	0.25	30.3
corr_V2_Q2	0.55	0.26	47.0
corr_V3_Q2	0.74	0.2	27.1
corr_V2_Q3	0.26	0.38	147
corr_V3_Q3	0.91	0.12	13.1
corr_V3_V2	0.35	0.34	96.3
<b>Error Model Parameters</b>			
b	0.21	0.0093	4.46

population value of 4.3h, a value in good agreement to the high range values estimated by NCA.

The distribution of residuals, scatter of residuals and correlation between predicted and measured concentrations plots (Figs. 5–7) indicated that the model adequately described the observed data with no systematic bias in predictions. Evaluation by pcVPC indicated overall good agreement for the 5th, median and 95th percentiles of LNA-i-miR-221 concentrations between observation and predictions (Fig. 7), supporting the conclusion that the final PK model provided a good description of the data.

The age of patients was the only covariate included in the model showing a strong correlation with V1 parameter (Fig. 2b) and because its inclusion in the model sensibly reduced both the OFV and BIC scores. Before using this covariate in the model, the values were normalized for the weighted mean of population, according to the formula  $\text{logtAge} = (\log(\text{Age}/62.4438))$ . Nevertheless, as V1 value could represent the blood

**Table 3b**

Predicted individual PK parameter values for LNA-i-miR-221.

	Cl	V1	Q2	V2	Q3	V3	term t1/2	Age	Individual_weight_kg	logtAge	logtIndividual_weight_kg
id	ml/h/kg	mL/kg	ml/h/kg	mL/kg	ml/h/kg	mL/kg	h	Y	kg		
2	160	120	470	120	99	830	4.64	74	70	0.17	0.026
4	210	50	480	150	120	1300	4.95	66	76	0.055	0.1
5	240	23	650	150	150	1500	4.83	55	58.5	-0.13	-0.15
6	190	59	640	210	95	1100	4.99	64	58	0.025	-0.16
7	250	60	840	250	160	2000	6.40	65	60	0.04	-0.13
9	230	52	600	170	170	1900	6.40	66	60	0.055	-0.13
10	250	68	680	250	88	1000	3.65	68	99	0.085	0.37
11	330	54	840	410	140	1800	4.76	65	67.5	0.04	-0.01
12	180	21	320	150	44	640	3.12	54	63.5	-0.15	-0.071
13	230	5.7	770	200	60	770	2.94	40	58	-0.45	-0.16
14	100	69	120	98	12	320	3.38	73	72	0.16	0.054
15	340	92	770	440	110	1500	4.14	74	43	0.17	-0.46
18	210	39	580	320	47	520	2.90	60	70	-0.04	0.026
19	160	28	330	210	31	610	3.67	56	108	-0.11	0.46
21	130	100	120	180	9.6	350	3.36	68	80	0.085	0.16

volume/kg of body weight, we do not find any obvious physiological correlation between these two factors. Taking in consideration that we used a dataset relatively small; it would be interesting to verify if this correlation may be confirmed within a larger population of patients.

### 3.3. Urine analysis

LNA-i-miR-221 levels were detectable in the urine of all patients in all cohorts up to two days after the last administration. This result suggests that the true terminal half-life of LNA-i-miR-221 can indeed be quite a bit longer than the apparent value measured from plasma profiles. As no changes in systemic clearance were observed following repeated administrations, the excretion of LNA-i-miR-221 in urine at the late time point after administration seems to be coherent with the systemic distribution and retention by tissues. Such processes normally involve surface protein interactions and endocytosis, which finally lead to cell internalization and a relatively slower excretion (Yu et al., 2013). Over the range of tested doses, data collected in urine indicated a progressive increase with predicted time of the LNA-i-miR-221 concentration eliminated by renal clearance, suggesting a potential, although moderate, accumulation during the investigated period in patients, evidently associated with a longer elimination half-life from tissues.

### 3.4. Predicted vs measured clearance values

Predicted human clearance values (Table 6a–b) were compared with the experimental averaged values obtained by combining all the clearance results measured on each PK occasion in human and for each subject. Distinct averages were only calculated per each dose level, as we observed (following initial NCA) a dose-depending trend in experimentally measured clearance values (Table 2). PopPK analysis suggested that this trend was mainly due to the poor estimation of the terminal elimination phase at lower dosing regimen and not to a non-linear PK of LNA-i-miR-221.

Among the different approaches applied for allometrically scaling the clearance of LNA-i-miR-221 measured in preclinical species to human (Di Martino et al., 2020), the “1-species (rat) allometric scaling” (see Eq. 4in reference (Di Martino et al., 2019)) gave the most accurate prediction. The approaches including species-specific plasma protein binding (PPB) correction were slightly but consistently more predictive than the analogue approaches with no correction, except for the “direct scaling with two species (rat and monkey)” (as per Eq.1in reference (Di Martino et al., 2019)) that was relatively insensitive to PPB correction (same predicted CL values with or without correction). Interestingly, this approach was the least accurate prediction of the four methods applied. In fact, renal excretion of oligonucleotides may be strongly impacted by their binding to plasma proteins. As detailed in our

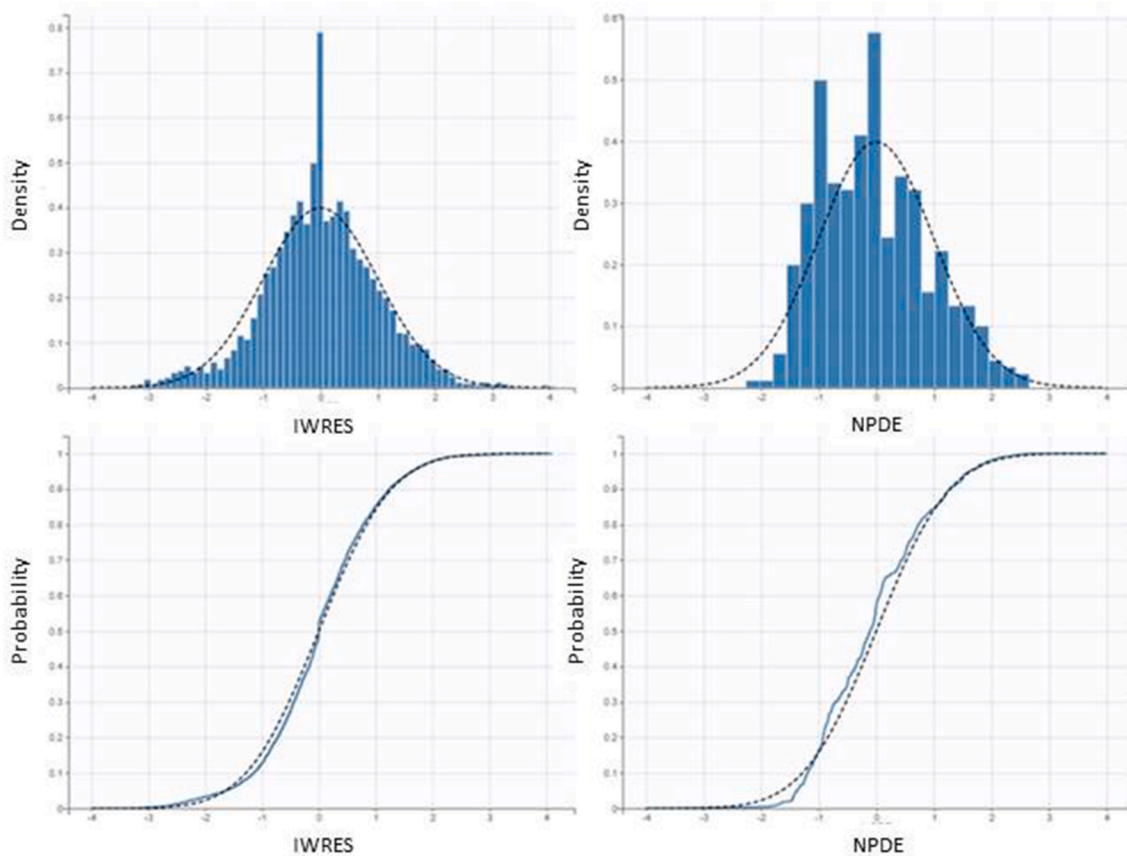


Fig. 5. Left plots: Individual weighed residuals (IWRS = estimates of the standardized residual ( $e_{ij}$ ) based on individual predictions). Right plots: Normalized prediction distribution errors (NPDE = Normalized Prediction Distribution Errors).

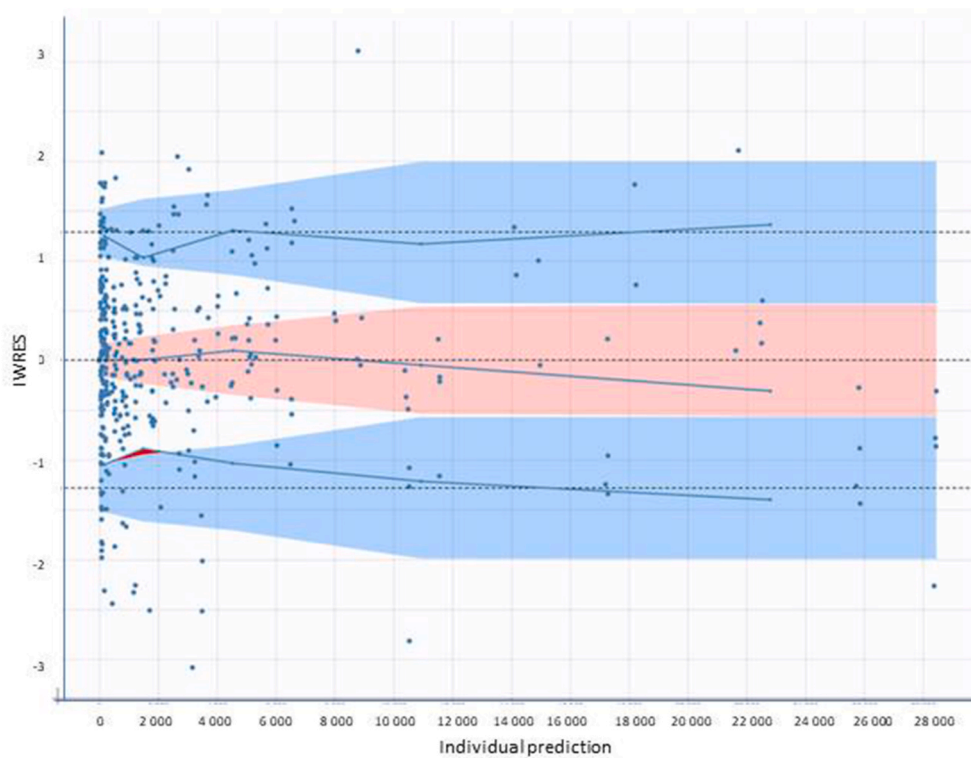


Fig. 6. Scatter plots of residuals including 90% prediction intervals (colored shaded areas). Blue lines represent empirical percentiles. (For interpretation of the references to color in this figure legend, the reader is referred to the Web version of this article.)

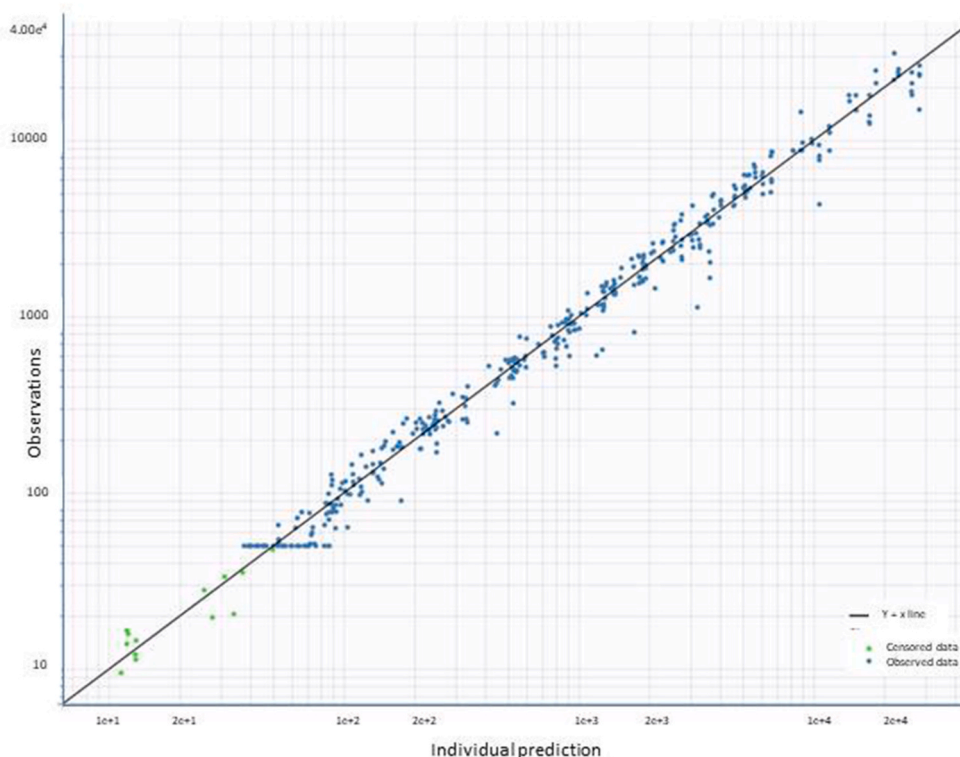


Fig. 7. Correlation between predicted (3 compartments – lin CL model) and measured individual concentrations of LNA-i-miR-221 in humans.

previous work (Di Martino et al., 2019, 2020) and reported in Table 4, protein binding values were relatively close across species, the moderately improved prediction seems to suggest that this factor could be important, but the impact is relatively mitigated by the similar free fraction values measured for LNA-i-miR-221 across the different species tested.

In general, all the allometric scaling approaches tended to underestimate in various degrees the clearance values in humans measured using the NCA approach. The errors spun from 5.2 to 2.6-fold under prediction, depending on the dose level, for the less predictive method, and from 2.3 to 1.2 folds underprediction for the method 1-species (rat) allometric scaling with PPB correction (Table 5). This last could be considered a reasonably well-predicted value. Clearly, the clearance values measured at the lower doses were less accurately predicted than the values at higher doses due to the apparent non-linear clearance measured in humans by applying the NCA approach.

Using the PopPK model approach, that doesn't assume any dose dependency for the CL value, the overall population value for this parameter (200 mL/min/kg) was predicted with less than 2-fold error by the 1-species (rat) allometric scaling with PPB correction method which confirmed to be the most predictive allometric formula for LNA-i-miR-221.

Table 4

Protein binding values for the test item in human, monkey and rat plasma. Data are presented as mean  $\pm$  standard deviation ( $n = 3$ ). Unbound fraction ( $f_u$ ) values (averages of the two tested concentrations) used for the unbound clearance estimation LNA-i-miR-221 concentration.

Species	1 $\mu$ M	10 $\mu$ M	Mean PPB	mean $f_u$
Human	98.6 $\pm$ 0.32 (%)	98.5 $\pm$ 0.09 (%)	98.55 (%)	0.0145
Monkey	98.2 $\pm$ 0.39 (%)	99.05 $\pm$ 0.39 (%)	98.63 (%)	0.0138
Rat	98.5 $\pm$ 0.17 (%)	98.9 $\pm$ 0.17 (%)	98.70 (%)	0.0130

Table 5

Comparison between predicted human clearance values for LNA-i-miR-221 and experimentally measured on patients during P1CT.

dose level	dose mg/kg/administration					
	0.5	1	2	3	5	
measured CL (avrg) (mL/h/kg)	274	310	309	250	157	
<b>(no PPB correction)</b>	predicted CL	measured/predicted ratio				
	ml/h/kg					
direct scaling 2-species (r, mk) (Eq.1)	60	4.57	5.16	5.15	4.16	2.62
Tang et al. method 2-species (r, mk) (Eq.3)	66	4.15	4.69	4.68	3.78	2.38
1-species (rat) allometric scaling (Eq.4)	114	2.40	2.72	2.71	2.19	1.38
1-species (mk) allometric scaling (Eq.4)	84	3.26	3.69	3.68	2.97	1.87
<b>(with PPB correction)</b>	predicted CL	measured/predicted ratio				
	ml/h/kg					
direct scaling 2-species (r, mk) (Eq.1)	60	4.57	5.16	5.15	4.16	2.62
Tang et al. method 2-species (r, mk) (Eq.3)	69	3.97	4.49	4.48	3.62	2.28
1-species (rat) allometric scaling (Eq.4)	132	2.08	2.35	2.34	1.89	1.19
1-species (mk) allometric scaling (Eq.4)	90	3.05	3.44	3.43	2.77	1.75

r = rat; mk = monkey.

#### 4. Discussion

We already discussed the rat NCA PK results used to initially scale the clearance in humans that were collected at a dose level of 12.5 mg/kg (Di Martino et al., 2019). When multiple dose levels were tested in rats,



**Table 6a**

Predicted LNA-i-miR-221 human PK parameters, based on total CLp using different allometric approaches.

	Total plasma clearance	AUC/Dose	AUC for 0.78 <sup>a</sup> mg/kg i. v. dose	AUC for 1.82 <sup>a</sup> mg/kg i. v. dose	AUC for 5.0 <sup>a</sup> mg/kg i. v. dose
allometric method used for prediction	mL/h/kg	h*ng/mL* (mg Dose) <sup>-1</sup>	h*ng/mL	h*ng/mL	h*ng/mL
direct scaling 2-species (r, mk) (Eq.1)	60	16264	12686	29600	81318
Tang et al. method 2-species (r, mk) (Eq.3)	66	15443	12046	28106	77215
1-species (rat) allometric scaling (Eq.4)	114	8643	6741	15730	43214
1-species (monkey) allometric scaling (Eq.4)	84	11711	9135	21315	58557
	Geom mean	Geom mean	Geom mean	Geom mean	Geom mean
	1.3	12627	9849	22981	63135

**Table 6b**

Predicted LNA-i-miR-221 human PK parameters, based on unbound CLpu using different allometric approaches.

	Total plasma clearance	AUC/Dose	AUC for 0.78 <sup>a</sup> mg/kg i. v. dose	AUC for 1.82 <sup>a</sup> mg/kg i. v. dose	AUC for 5.0 <sup>a</sup> mg/kg i. v. dose
allometric method used for prediction	mL/h/kg	h*ng/mL* (mg Dose) <sup>-1</sup>	h*ng/mL	h*ng/mL	h*ng/mL
direct scaling 2-species (r, mk) (Eq.1)	60	16386	12781	29823	81931
Tang et al. method 2-species (r, mk) (Eq.3)	69	14462	11280	26320	72309
1-species (rat) allometric scaling (Eq.4)	132	7749	6044	14103	38743
1-species (mk) allometric scaling (Eq.4)	90	11106	8662	20212	55528
	Geom mean	Geom mean	Geom mean	Geom mean	Geom mean
	1.4	11950	9321	21749	59750

m = mouse, r = rat, mk = monkey.

<sup>a</sup> HED predicted according to Eq.2; human PAD predicted according to Eq.5; assuming hum NOAEL = rat NOAEL.

we also observed an apparent dose dependent non-linear PK in this species, similarly to the human PK case, with a drug elimination mechanism apparently reaching a more constant value as the dose level increased.

This apparent non-linear behavior cannot be justified with saturable plasma protein binding as the renal clearance contribution would eventually increase and not decrease by increasing the fraction unbound

and because we observed no changes in plasma protein binding values, in all species, when LNA-i-miR-221 concentration was tested at 1 and 10  $\mu$ M (Table 5 and (Di Martino et al., 2020)).

Necessarily, for safety reasons, the initially tested dose in humans was lower than the NOAEL in rat and was scaled up progressively to the actual highest dose administered in the phase I study (5 mg/kg).

There is a clear linear dependency between the CL value in rat and the predicted CL in human based on the Eq. 4 (Di Martino et al., 2019), which means that the experimental value chosen in the rat PK-based scaling approach will proportionally impact the predicted value in man. As in the rat the average clearance value at NOAEL was 1.39 folds higher than the corresponding value observed at 12.5 mg/kg, the predicted human clearance based on this lower dose level in rat would have been proportionally higher. In this second scenario, the human clearance at 0.5 mg/mL value would have been even better predicted (within less than 2 folds difference with and without PPB correction), then rat clearance value at NOAEL would be the more appropriate choice to escalate the clearance in human to doses close to the HED, when we use NCA for estimating the clearance.

The measured plasma exposure of LNA-i-miR-221 in humans at the dose of 2 mg/kg, which is the administered dose closest to the previously predicted pharmacodynamic active dose in humans (PAD = 1.8 mg/kg), is notably close to the exposure in mice at 25 mg/kg (AUC<sub>0-inf,obs</sub> = 3226 h\*ng/mL) that was the measured effective exposure in the pre-clinical animal model and the corresponding dose was used to estimate the PAD in human.

Our comparative analysis between previously reported allometric prediction of LNA-i-miR-221 clearance in human and the experimentally measured clearance values in humans, showed that the most accurate prediction was achieved by applying the single species allometric scaling approach based on rat PK, following (eq. 4(Di Martino et al., 2019)) initially proposed by Tang et al.(Tang et al., 2007).

Several recent studies have suggested that single-species allometric scaling from monkeys is the superior way to predict the human PK of PS-ASOs (Nanavati et al., 2021; Y. Wang et al., 2019; Yu et al., 2015). Specifically, Imai et al. (2023) have investigated a phosphorodiamidate morpholino oligomers in mice, rats, cynomolgus monkeys, and dogs and used the results to extrapolate to humans by several methods. The authors estimated that human PK parameters and profiles, determined from cynomolgus monkeys by an allometric scaling approach, were the most suitable. We have recently published a similar work investigating the applicability of different allometric scaling approaches to human PK prediction for LNA-i-miR-221 (Di Martino et al., 2019). All the above reported studies, obtained the most accurate prediction of human CL<sub>tot</sub> by 1-species allometry from cynomolgus monkey with an exponent of 1 rather than the exponent of 0.75 as originally suggested by Tang and used by us in our approach for rat allometric scaling (CL<sub>tot</sub>, human = CL<sub>tot</sub>, animal\*(human weight/animal weight)<sup>b</sup>, where b = 1 or 0.75).

LNA-i-miR-221 hum CL estimation by scaling the cynomolgus monkey CL using the exponent of 1, shows improved prediction indeed and becomes comparable to rat-scaled CL (scaled with exponent = 0.75). For the higher dose in human (5 mg/kg), using the single species PPB correction approach, the ratio CL<sub>meas</sub> (NCA analysis)/CL predicted is 0.72 for cynomolgus monkey vs 1.12 using the rat CL based extrapolation with exponent of 0.75. According to this new comparative analysis, rat extrapolation remains still slightly better for our model but basically equivalent to cynomolgus monkey estimation. This is also confirmed by the fact that, for lower doses, the accuracy of rat vs cynomolgus monkey-based scaling approach showed in some cases an inversed accuracy ranking (for instance, using the measured hum CL = 200 mL/h/kg, estimated using the compartmental Pop PK approach from clinic data, the ratio CL<sub>meas</sub>/CL<sub>pred</sub> = 1.75 for rat-scaled CL and 0.97 for monkey-scaled CL, which is the most accurate prediction using monkey data).

In the recent past, several different authors have reported that the use of more than one species in allometric scaling to predict therapeutic proteins PK would not necessarily generate the best prediction(Ling

et al., 2009; W. Wang and Prueksaritanont, 2010). Our LNA-i-miR-221 studies seem to suggest that this conclusion may be extended also to the PK estimation of oligonucleotides.

Independently of the scaling equation we applied, the best predictions was obtained by applying the correction for the species-specific free drug fraction in plasma; this finding confirms what observed in previous similar investigations(Lombardo et al., 2013).

The LNA-i-miR-221 NCA PK parameters in rat were found to be predictive of the human NCA PK parameters, and consistently to what observed in human NCA, rat PK results showed an apparent dose dependency as well. Whether this effect is real or apparently due to the bioanalytical method sensitivity, this finding reinforces our confidence that the rat may be considered a good animal model for the PK analysis of LNA-i-miR-221 and other oligonucleotides in human.

Due to similar PPB values across species, renal CL in humans is a minor route of CL similarly to what previously observed in rat and monkeys, where a low percentage of dose was excreted unchanged in urines.

The mechanism behind the slow distribution of LNA-i-miR-221 in tissues has not been yet clarified. Liver is one of the organs in which oligonucleotides tend to preferentially distribute after administration (Roberts et al., 2020). Recent studies demonstrate that at least two distinct pathways are operant by which antisense oligonucleotides (ASO) accumulate in liver cells. We refer to these as a productive and a non-productive uptake pathway. The productive uptake pathway, which delivers ASO to the RNA cellular compartment, accounts for <20% of the total ASO delivered to liver tissue. Koller et al. suggested that the non-productive uptake pathway, accounting for the bulk ASO accumulating in cells is saturable and the ASO does not appear to have access to the target RNA(Koller et al., 2011). More recent works indicate that adsorption of PS-ASOs to the cell surface is rapid, does not require energy, and can be saturated. This suggests that ASOs can compete for association with specific membrane proteins and the competition may in turn result in productive internalization (Crooke et al., 2017; S. Wang et al., 2018).

Assuming a saturable uptake also for LNA-i-miR-221, a saturable clearance from plasma compartment could be expected with increasing doses. Since PS-ASOs are known to have a much higher propensity for protein binding than other ASOs, this difference may also increase the binding to cell membrane proteins. Despite of that, our analysis could not confirm the evidence of non-linear PK behaviour for LNA-i-miR-221 in human.

Clinical success can often be correlated with achieved tissue targeting and adequate cell penetration, and these remain major obstacles in the oligonucleotide field. Over the last 15 years, a great effort has been undertaken in both academic and industrial labs to gain a mechanistic understanding of how RNA therapeutics are internalized by cells(S. Wang et al., 2018). This analysis remains nevertheless challenging with the difficulty to distinguish total cellular uptake from methods that can more specifically measure penetration to the cytosol or nucleus(S. Wang et al., 2018; W. Wang and Prueksaritanont, 2010). Often, RNA therapeutics are observed to be taken up by cells, but still do not exert a change in mRNA levels or protein expression ('non-productive uptake').

Nowadays, it has been made clear that more than 50% of miRNA genes are located in cancer-associated genomic regions or in fragile sites, thus indicating that miRNAs may play a key role in the pathogenesis of human cancer(Di Martino et al., 2021; Gallo Cantafio et al., 2018; Ling et al., 2009). The expression pattern seems to be tissue specific. It has been also reported that different cell types have differing ASO-binding abilities(S. Wang et al., 2018).

In this context, it would be important, to better clarify the nature of therapeutic miRNAs like LNA-i-miR-221 tissues distribution and their intracellular 'productive uptake' capacity (uptake that leads to a phenotypic effect) by correlating the PK of LNA-i-miR-221 and its tissue and intracellular distribution level ( $\mu$ PK) (Pendergraft et al., 2020) to its effect and efficacy in patients (i.e. by ( $\mu$ )PK/PD modelling and/or QSP approaches).

## 5. Conclusions

Here we have presented an in-depth analysis (NCA and CA) of the human PK of LNA-i-miR-221. In vivo measured clearance values were compared with our initial predictions.

Our conclusive observations support that the single-species allometry may be more predictive versus multiple species allometric approaches in the PK estimation of oligonucleotides, as recently reported also for therapeutic proteins. Finally, our investigation for LNA-i-miR-221 suggests that using rat PK to anticipate CL in humans can indeed be a valid alternative to the use of non-human primates.

The predictive approach here discussed was found accurate not only in predicting the main PK parameters in human but suggesting the range of effective and safe dose to be applied in the next clinic phase 2. The evidence of primary and secondary target modulation of LNA-i-miR-221 and the low-grade side effects reported during the study confirmed that the preclinical data were correctly and safely scaled in human. Despite of this clearly important result, there are still evident gaps to be filled to achieve a complete mechanistic understanding of the PK and PK/PD behavior of oligonucleotides in vivo, which would probably benefit of  $\mu$ PK/PD and PBPK analysis, detailing the concentration of therapeutics oligonucleotides at the targeted region, cell type, and organelle, as we have discussed here.

## Funding information

This work was supported by the Italian Association for Cancer Research (AIRC), PI: PT. "Special Program Molecular Clinical Oncology-5 per mille" n. 9980, 2010/15 and its Extension Program 2016/17 n.9980.

## CRediT authorship contribution statement

**Massimiliano Fonsi:** Conceptualization, Visualization, Writing – review & editing, Data curation, Methodology, and, Formal analysis. **Jacques Fulbert:** Methodology, and, Formal analysis, Data curation. **Pierre-Andre Billat:** Methodology, and, Formal analysis, Data curation. **Mariamena Arbitrio:** Supervision. **Pierosandro Tagliaferri:** Writing – review & editing. **Pierfrancesco Tassone:** Writing – review & editing, Funding acquisition. **Maria Teresa Di Martino:** Conceptualization, Visualization, Writing – review & editing, Data curation, Methodology, and, Formal analysis, Supervision.

## Declaration of competing interest

The authors declare that they have no known competing financial interests or personal relationships that could have appeared to influence the work reported in this paper.

## Data availability

Data will be made available on request.

## Acknowledgments

Joanna Moore, ELS (Charles River) provided editorial services in the manuscript development.

## References

- Caracciolo, D., Di Martino, M.T., Amodio, N., Morelli, E., Montesano, M., Botta, C., Tassone, P., 2019. miR-22 suppresses DNA ligase III addiction in multiple myeloma. *Leukemia* 33 (2), 487–498. <https://doi.org/10.1038/s41375-018-0238-2>.
- Crooke, S.T., Wang, S., Vickers, T.A., Shen, W., Liang, X.H., 2017. Cellular uptake and trafficking of antisense oligonucleotides. *Nat. Biotechnol.* 35 (3), 230–237. <https://doi.org/10.1038/nbt.3779>.



- Di Martino, M.T., Arbitrio, M., Caracciolo, D., Cordua, A., Cuomo, O., Grillone, K., Tassone, P., 2022. miR-221/222 as biomarkers and targets for therapeutic intervention on cancer and other diseases: a systematic review. *Mol. Ther. Nucleic Acids* 27, 1191–1224. <https://doi.org/10.1016/j.omtn.2022.02.005>.
- Di Martino, M.T., Arbitrio, M., Caracciolo, D., Scionti, F., Tagliaferri, P., Tassone, P., 2020. Dose-finding study and pharmacokinetics profile of the novel 13-mer antisense miR-221 inhibitor in sprague-dawley rats. *Mol. Ther. Nucleic Acids* 20, 73–85. <https://doi.org/10.1016/j.omtn.2020.01.036>.
- Di Martino, M.T., Arbitrio, M., Fonsi, M., Erratico, C.A., Scionti, F., Caracciolo, D., Tassone, P., 2019. Allometric scaling approaches for predicting human pharmacokinetic of a locked nucleic acid oligonucleotide targeting cancer-associated miR-221. *Cancers* 12 (1). <https://doi.org/10.3390/cancers12010027>.
- Di Martino, M.T., Campani, V., Misso, G., Gallo Cantafio, M.E., Gulla, A., Foresta, U., Caraglia, M., 2014a. In vivo activity of miR-34a mimics delivered by stable nucleic acid lipid particles (SNALPs) against multiple myeloma. *PLoS One* 9 (2), e90005. <https://doi.org/10.1371/journal.pone.0090005>.
- Di Martino, M.T., Gulla, A., Cantafio, M.E., Lionetti, M., Leone, E., Amodio, N., Tassone, P., 2013. In vitro and in vivo anti-tumor activity of miR-221/222 inhibitors in multiple myeloma. *Oncotarget* 4 (2), 242–255. <https://doi.org/10.18632/oncotarget.820>.
- Di Martino, M.T., Gulla, A., Gallo Cantafio, M.E., Altomare, E., Amodio, N., Leone, E., Tassone, P., 2014b. In vitro and in vivo activity of a novel locked nucleic acid (LNA)-inhibitor-miR-221 against multiple myeloma cells. *PLoS One* 9 (2), e89659. <https://doi.org/10.1371/journal.pone.0089659>.
- Di Martino, M.T., Leone, E., Amodio, N., Foresta, U., Lionetti, M., Pitari, M.R., Tassone, P., 2012. Synthetic miR-34a mimics as a novel therapeutic agent for multiple myeloma: in vitro and in vivo evidence. *Clin. Cancer Res.* 18 (22), 6260–6270. <https://doi.org/10.1158/1078-0432.CCR-12-1708>.
- Di Martino, M.T., Riillo, C., Scionti, F., Grillone, K., Polera, N., Caracciolo, D., Tassone, P., 2021. miRNAs and lncRNAs as novel therapeutic targets to improve cancer immunotherapy. *Cancers* 13 (7). <https://doi.org/10.3390/cancers13071587>.
- Di Martino, M.T., Rossi, M., Caracciolo, D., Gulla, A., Tagliaferri, P., Tassone, P., 2016. Mir-221/222 are promising targets for innovative anticancer therapy. *Expert Opin. Ther. Targets* 20 (9), 1099–1108. <https://doi.org/10.1517/14728222.2016.1164693>.
- Franzoni, S., Morbioli, L., Turtoro, A., Solazzo, L., Greco, A., Arbitrio, M., Breda, M., 2020. Development and validation of bioanalytical methods for LNA-i-miR-221 quantification in human plasma and urine by LC-MS/MS. *J. Pharm. Biomed. Anal.* 188, 113451. <https://doi.org/10.1016/j.jpba.2020.113451>.
- Franzoni, S., Vezzelli, A., Turtoro, A., Solazzo, L., Greco, A., Tassone, P., Breda, M., 2018. Development and validation of a bioanalytical method for quantification of LNA-i-miR-221, a 13-mer oligonucleotide, in rat plasma using LC-MS/MS. *J. Pharm. Biomed. Anal.* 150, 300–307. <https://doi.org/10.1016/j.jpba.2017.12.027>.
- Gallo Cantafio, M.E., Grillone, K., Caracciolo, D., Scionti, F., Arbitrio, M., Barbieri, V., Di Martino, M.T., 2018. From single level analysis to multi-omics integrative approaches: a powerful strategy towards the precision Oncology. *High Throughput* 7 (4). <https://doi.org/10.3390/ht7040033>.
- Gallo Cantafio, M.E., Nielsen, B.S., Mignogna, C., Arbitrio, M., Botta, C., Frandsen, N.M., Di Martino, M.T., 2016. Pharmacokinetics and pharmacodynamics of a 13-mer LNA-inhibitor-miR-221 in mice and non-human primates. *Mol. Ther. Nucleic Acids* 5 (6). <https://doi.org/10.1038/mtna.2016.36>.
- Gulla, A., Di Martino, M.T., Gallo Cantafio, M.E., Morelli, E., Amodio, N., Botta, C., Tassone, P., 2016. A 13 mer LNA-i-miR-221 inhibitor restores drug sensitivity in melphalan-refractory multiple myeloma cells. *Clin. Cancer Res.* 22 (5), 1222–1233. <https://doi.org/10.1158/1078-0432.CCR-15-0489>.
- Imai, S., Suda, Y., Mori, J., Sasaki, Y., Yamada, T., Kusano, K., 2023. Prediction of human pharmacokinetics of phosphorodiamidate morpholino oligonucleotides in duchenne muscular dystrophy patients using viltolarsen. *Drug Metab. Dispos.* 51 (10), 1428–1435. <https://doi.org/10.1124/dmd.123.001425>.
- Koller, E., Vincent, T.M., Chappell, A., De, S., Manoharan, M., Bennett, C.F., 2011. Mechanisms of single-stranded phosphorothioate modified antisense oligonucleotide accumulation in hepatocytes. *Nucleic Acids Res.* 39 (11), 4795–4807. <https://doi.org/10.1093/nar/gkr089>.
- Ling, J., Zhou, H., Jiao, Q., Davis, H.M., 2009. Interspecies scaling of therapeutic monoclonal antibodies: initial look. *J. Clin. Pharmacol.* 49 (12), 1382–1402. <https://doi.org/10.1177/0091270009337134>.
- Lombardo, F., Waters, N.J., Argikar, U.A., Dennehy, M.K., Zhan, J., Gunduz, M., Obach, R.S., 2013. Comprehensive assessment of human pharmacokinetic prediction based on in vivo animal pharmacokinetic data, part 2: clearance. *J. Clin. Pharmacol.* 53 (2), 178–191. <https://doi.org/10.1177/0091270012440282>.
- Misso, G., Zappavigna, S., Castellano, M., De Rosa, G., Di Martino, M.T., Tagliaferri, P., Caraglia, M., 2013. Emerging pathways as individualized therapeutic target of multiple myeloma. *Expert Opin. Biol. Ther.* 13 (Suppl. 1), S95–S109. <https://doi.org/10.1517/14712598.2013.807338>.
- Morelli, E., Biomonte, L., Federico, C., Amodio, N., Di Martino, M.T., Gallo Cantafio, M.E., Tassone, P., 2018. Therapeutic vulnerability of multiple myeloma to MIR17PT1, a first-in-class inhibitor of pri-miR-17-92. *Blood* 132 (10), 1050–1063. <https://doi.org/10.1182/blood-2018-03-836601>.
- Morelli, E., Leone, E., Cantafio, M.E., Di Martino, M.T., Amodio, N., Biomonte, L., Tassone, P., 2015. Selective targeting of IRF4 by synthetic microRNA-125b-5p mimics induces anti-multiple myeloma activity in vitro and in vivo. *Leukemia* 29 (11), 2173–2183. <https://doi.org/10.1038/leu.2015.124>.
- Nanavati, C., McMullen, G., Yu, R., Geary, R.S., Henry, S.P., Wang, Y., 2021. Interspecies scaling of human clearance and plasma trough exposure for antisense oligonucleotides: a retrospective analysis of GalNAc3-conjugated and unconjugated-antisense oligonucleotides. *Nucleic Acid Therapeut.* 31 (4), 298–308. <https://doi.org/10.1089/nat.2020.0911>.
- Pendergraff, H., Schmidt, S., Vikesa, J., Weile, C., Overup, C., M, W.L., Koch, T., 2020. Nuclear and cytoplasmic quantification of unconjugated, label-free locked nucleic acid oligonucleotides. *Nucleic Acid Therapeut.* 30 (1), 4–13. <https://doi.org/10.1089/nat.2019.0810>.
- Roberts, T.C., Langer, R., Wood, M.J.A., 2020. Advances in oligonucleotide drug delivery. *Nat. Rev. Drug Discov.* 19 (10), 673–694. <https://doi.org/10.1038/s41573-020-0075-7>.
- Rossi, M., Amodio, N., Di Martino, M.T., Caracciolo, D., Tagliaferri, P., Tassone, P., 2013. From target therapy to miRNA therapeutics of human multiple myeloma: theoretical and technological issues in the evolving scenario. *Curr. Drug Targets* 14 (10), 1144–1149. Retrieved from. <http://www.ncbi.nlm.nih.gov/pubmed/23834146>.
- Rossi, M., Amodio, N., Di Martino, M.T., Tagliaferri, P., Tassone, P., Cho, W.C., 2014. MicroRNA and multiple myeloma: from laboratory findings to translational therapeutic approaches. *Curr. Pharmaceut. Biotechnol.* 15 (5), 459–467. Retrieved from. <http://www.ncbi.nlm.nih.gov/pubmed/24846067>.
- Santolla, M.F., Lappano, R., Cirillo, F., Rigracciolo, D.C., Sebastiani, A., Abonante, S., Vivacqua, A., 2018. miR-221 stimulates breast cancer cells and cancer-associated fibroblasts (CAFs) through selective interference with the A20/c-Rel/CTGF signaling. *J. Exp. Clin. Cancer Res.* 37 (1), 94. <https://doi.org/10.1186/s13046-018-0767-6>.
- Tang, H., Hussain, A., Leal, M., Mayersohn, M., Fluhler, E., 2007. Interspecies prediction of human drug clearance based on scaling data from one or two animal species. *Drug Metab. Dispos.* 35 (10), 1886–1893. <https://doi.org/10.1124/dmd.107.016188>.
- Tassone, P., Di Martino, M.T., Arbitrio, M., Fiorillo, L., Staropoli, N., Ciliberto, D., Tagliaferri, P., 2023. Safety and activity of the first-in-class locked nucleic acid (LNA) miR-221 selective inhibitor in refractory advanced cancer patients: a first-in-human, phase 1, open-label, dose-escalation study. *J. Hematol. Oncol.* 16 (1), 68. <https://doi.org/10.1186/s13045-023-01468-8>.
- Wang, S., Allen, N., Vickers, T.A., Revenko, A.S., Sun, H., Liang, X.H., Crooke, S.T., 2018. Cellular uptake mediated by epidermal growth factor receptor facilitates the intracellular activity of phosphorothioate-modified antisense oligonucleotides. *Nucleic Acids Res.* 46 (7), 3579–3594. <https://doi.org/10.1093/nar/gky145>.
- Wang, W., Prueksaranont, T., 2010. Prediction of human clearance of therapeutic proteins: simple allometric scaling method revisited. *Biopharm Drug Dispos.* 31 (4), 253–263. <https://doi.org/10.1002/bdd.708>.
- Wang, Y., Yu, R.Z., Henry, S., Geary, R.S., 2019. Pharmacokinetics and clinical pharmacology considerations of GalNAc(3)-conjugated antisense oligonucleotides. *Expert Opin. Drug Metabol. Toxicol.* 15 (6), 475–485. <https://doi.org/10.1080/17425255.2019.1621838>.
- Yu, R.Z., Grundy, J.S., Geary, R.S., 2013. Clinical pharmacokinetics of second generation antisense oligonucleotides. *Expert Opin. Drug Metabol. Toxicol.* 9 (2), 169–182. <https://doi.org/10.1517/17425255.2013.737320>.
- Yu, R.Z., Grundy, J.S., Henry, S.P., Kim, T.W., Norris, D.A., Burkey, J., Geary, R.S., 2015. Predictive dose-based estimation of systemic exposure multiples in mouse and monkey relative to human for antisense oligonucleotides with 2'-o-(2-methoxyethyl) modifications. *Mol. Ther. Nucleic Acids* 4 (1), e218. <https://doi.org/10.1038/mtna.2014.69>.